AFGL-TR-81-0134

PROOF OF CONCEPT STUDY

A. S. Zachor, F. P. DelGreco and Lt. M. Ahmadjian

Atmospheric Radiation Consultants, Inc.
59 High Street
Acton, Massachusetts   01720

March 1981

Scientific Report No. 6

AIR FORCE GEOPHYSICS LABORATORY
AIR FORCE SYSTEMS COMMAND
UNITED STATES AIR FORCE
HANSCOM AFB, MASSACHUSETTS   01731

A

81 9 18 114

REPORT DOCUMENTATION PAGE	READ INSTRUCTIONS BEFORE COMPLETING FORM

1. REPORT NUMBER	2. GOVT ACCESSION NO.	3. RECIPIENT'S CATALOG NUMBER
AFGL-TR-81-0134	AD-A104 338	

4. TITLE (and Subtitle)	5. TYPE OF REPORT & PERIOD COVERED
PROOF OF CONCEPT STUDY	Scientific Report No. 6
	6. PERFORMING ORG. REPORT NUMBER

7. AUTHOR(s)	8. CONTRACT OR GRANT NUMBER(s)
A. S. Zachor F. P. DelGreco M. Ahmadjian	F19628-77-C-0203 U.S.U. Subcontract No. SC-80-056

9. PERFORMING ORGANIZATION NAME AND ADDRESS	10. PROGRAM ELEMENT, PROJECT, TASK AREA & WORK UNIT NUMBERS
Atmospheric Radiation Consultants, Inc. 59 High Street Acton, Massachusetts 01720	61102F 2310G101

11. CONTROLLING OFFICE NAME AND ADDRESS	12. REPORT DATE
Air Force Geophysics Laboratory (OPR) Hanscom AFB, MA 01731 Contract Monitor: Dean Kimball (OPR)	23 March 1981
	13. NUMBER OF PAGES
	38

14. MONITORING AGENCY NAME & ADDRESS(if different from Controlling Office)	15. SECURITY CLASS. (of this report)
	UNCLASSIFIED
	15a. DECLASSIFICATION/DOWNGRADING SCHEDULE

16. DISTRIBUTION STATEMENT (of this Report)

Approved for public release; distribution unlimited.

17. DISTRIBUTION STATEMENT (of the abstract entered in Block 20, if different from Report)

18. SUPPLEMENTARY NOTES

*AIR FORCE GEOPHYSICS LABORATORY

19. KEY WORDS (Continue on reverse side if necessary and identify by block number)

IR remote sensing, spectral correlation, correlation detection, trace gas detection, spectroscopy, high spectral resolution, least-squares estimation

20. ABSTRACT (Continue on reverse side if necessary and identify by block number)

Field test data were analyzed and computer simulations performed to validate the predictions of an earlier study, which calculated the minimum detectable quantities (MDQ's) of trace gases that can be detected remotely using high-resolution spectroscopy. The study demonstrates convincingly that reliable detection can be achieved near the MDQ level in a benign real-world environment.

DD FORM 1473   EDITION OF 1 NOV 65 IS OBSOLETE

TABLE OF CONTENTS

SECTION 1
INTRODUCTION AND SUMMARY

A localized cloud containing gases that have infrared absorption bands, e.g., the chemical effluent of a stationary source, can be detected on the basis of the contrast it produces in an IR scene image. Obvious requirements in this method of remote detection are that the cloud temperature is different from the background brightness temperature and that the resultant spatial radiance contrast is distinguishable from background clutter.

Resolution of the IR image into many spectral elements will enhance the ability of the system to distinguish between different target species having overlapping spectral bands and/or to suppress the effects of interferences, particularly those resulting from spatial and temporal variations in atmospheric spectral absorption and background emission.

The detection concept addressed by this study is pictured in Fig. 1. A scene that includes a chemical effluent cloud is viewed by an airborne spectrometer having a mosaic of detectors, some of which see the target cloud-plus-background and others that see only the background. The difference in the outputs of two appropriately selected detectors gives the spectral radiance contrast between the target cloud and the background. Comparison of the measured contrast spectrum and a computed reference contrast spectrum can be used to identify the presence of a particular trace gas, and also to
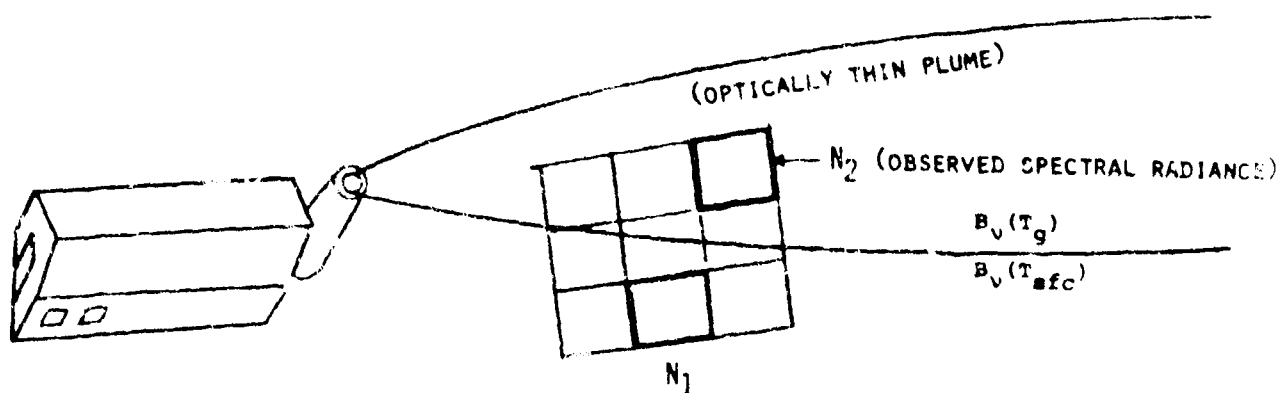

(OPTICALLY THIN PLUME)

N_2 (OBSERVED SPECTRAL RADIANCE)

$B_\nu(T_g)$

$B_\nu(T_{sfc})$

N_1

Figure 1. Detection scenario

1

estimate its "detectable quantity". Detection and quantification involve simple least-squares estimation procedures developed in a previous study[1] and reviewed in Section 2. The detectable (observable) quantity of the target trace gas is essentially the product of its molecular column thickness in the line-of-sight and the Planck spectral radiance difference corresponding to the temperature difference between the target gas and background. The minimum detectable quantity (MDQ) will be defined as the value that corresponds to approximately 95 percent probability of detection and one percent probability of false detection. The MDQ depends on the noise equivalent spectral radiance (NESR) of the spectrometer system, the variance of the reference contrast spectrum and the number of resolved spectral elements in the detection band.

Of course, in some applications it may be desirable or necessary to remotely infer both the target gas column thickness and its temperature. In principle, these quantities can be determined by more detailed analysis of the observed contrast spectral radiance, but it is not possible to specify detection limits and accuracies without further study of the problem. Knowledge of the predicted MDQ can be used at least to determine whether particular combinations of target gas column thickness and gas-background temperature difference will be detectable in a given scenario.

A previous study[1] by Atmospheric Radiation Consultants, Inc. (ARC) established baseline design configurations for an airborne Fourier Transform Spectrometer (FTS) detection system with modest-sized foreoptics. The study determined the NESR of one of the baseline systems and the corresponding MDQ's for the 15 species $C_2H_4O_2$, CH_4, CH_3I, CO, CO_2, DF, HBr, HCl, HF, HI, HNO_3, NH_3, N_2O, NO_2 and SO_2. The MDQ results given in Ref. 1 assume that the target cloud is viewed in the direction of the nadir from an altitude above most of the absorbing atmosphere. (These results and the detection concept are also summarized in two papers; cf. Zachor, et al[2,3]).

The choice of an FTS system over a grating spectrometer system for this application is supported by a study performed by SSG, Inc.[4] The basic radiometric design requirements and tradeoffs were established in an earlier study[5] by Bartlett Systems, inc.

2

The PROOF OF CONCEPT TESTING program consisted of laboratory/field tests and data analyses by Utah State University, ARC and the Aerospace Corporation. The purpose of the USU Electrodynamics Laboratory and ARC efforts was to validate the detection concept and theoretical prediction models of Ref. 1 through field tests and subsequent data analysis, as well as through computer simulation. ARC was also charged with investigating methods for obtaining separate estimates of the target gas column thickness and temperature.

The field tests were performed by USU, with guidance from AFGL personnel. A model stack emitting a controlled flow of ambient-temperature N_2O in front of a heated "background" plate was observed by an FTS system at a distance of 273 meters. The source and detection system were both at ground level. The side walls of the "three-wall" model stack limited the expansion of the stack effluent and reduced the effects of wind. It was determined by USU that the N_2O concentration (and column thickness) observed by the FTS system could be reliably controlled by metering the N_2O supply to the stack. Interferograms were recorded for N_2O-plus-background (supply ON) and for background only (supply OFF). USU reduced the inferferograms to spectra and supplied these to ARC for analysis. They also supplied appropriate meteorological data and the background plate temperature. From these data ARC computed the reference contrast spectrum, the system NESR, the MDQ and corresponding detection threshold quantity, the detection decision (yes or no), the detectable quantity present and the corresponding volumn concentration of N_2O. Afterwards, the inferred concentrations were compared to values supplied by USU.

The detection band selected for the experiment is 2170-2260 cm^{-1}, which includes most of the v_3 band of N_2O (this is a good choice for the field tests, but not the optimum oectral band for detection of N_2O from a high-altitude platform[1]). Atmospheric N_2O and the isotope $C^{13}O_2^{16}$ produce significant absorptions over a 273-meter ground-level path in the selected band. Thus, the tests included the effects of atmospheric attenuation, even though the path length was short. Detection near the MDQ level implies very low signal to noise in the measured contrast radiance spectrum. The field tests were designed primarily to verify that reliable detection could be achieved at, or slightly above, the MDQ level, in a benign real-world environment.

The computer simulation performed by ARC utilized a single pair of USU measurements representing a contrast radiance spectrum of high signal-to-noise. The computer was used essentially to add pseudo-random noise, i.e., to degrade the S/N, or equivalently, to raise the MDQ level to the detectable quantity present during the USU high-S/N measurement. The resultant noisy contrast spectra were analyzed in the same way as contrast spectra obtained from pairs of USU low-S/N measurements. The noise-addition process was performed on the computer one thousand times. From the number of successful detections it was verified that the detection probability was approximately 95 percent. Similar computations involving noise-only spectra were used to verify that the false detection probability was approximately one percent.

This final report summarizes ARC's efforts in the PROOF OF CONCEPT TESTING program. Details of the field tests, the three-wall stack, the FTS system used in the tests, reduction of inferferograms, etc. are contained in USU's final report.

The remainder of Section 1 gives a sample of the results obtained and the conclusions of the ARC study. Section 2 reviews the theoretical basis of the concept and the spectral analysis methods. Sections 3 through 5 contain additional results and a more detailed account of the simulation and data analysis efforts.

1.1 Sample of Results

The spectral radiance data for each field test was supplied by USU as a digital tape which usually contained 12 consecutive target spectra (N_2O supply on), 12 corresponding background spectra (N_2O supply off), and two spectral responsivity runs. The N_2O flow rate was held constant in each series of 12 target runs, except during the test of 19 February 1981, when it was purposely varied.

Figure 2 compares the N_2O concentrations that were deduced by ARC from spectral analysis of the 19 February data to those measured by USU (from the calibrated flow meter). The analysis procedure is capable of providing estimates of only the detectable quantity, but knowledge of the ambient (N_2O) temperature and pressure, the background temperature and physical length of

4

the line-of-sight through the N_2O allowed a conversion to N_2O volumn concentration (ppmV units). It is seen that the actual concentration decreased between runs 1 and 6, then underwent a symmetrical increase between runs 6 and 11, and finally decreased from run 11 to run 12. The figure shows that N_2O was successfully detected in the eight runs for which the actual concentration was above the theoretical detection threshold; in the remaining four cases it was not detected (there were no false detections). Moreover, the differences between the deduced and measured values are within the theoretical + one-sigma uncertainty in the deductions.[*] Note that two successful detections were made very near the MDQ level of 17.8 ppmV $= 1.4 \times 10^{10}$ (molec/cm^2)(W/cm^2 sr cm^{-1}).

The constant flow rates used by USU in the other series of measurements corresponded to concentrations ranging from approximately 1.5 to 4 times the MDQ concentration. Very good agreement between inferred and measured concentrations was also obtained for these cases.
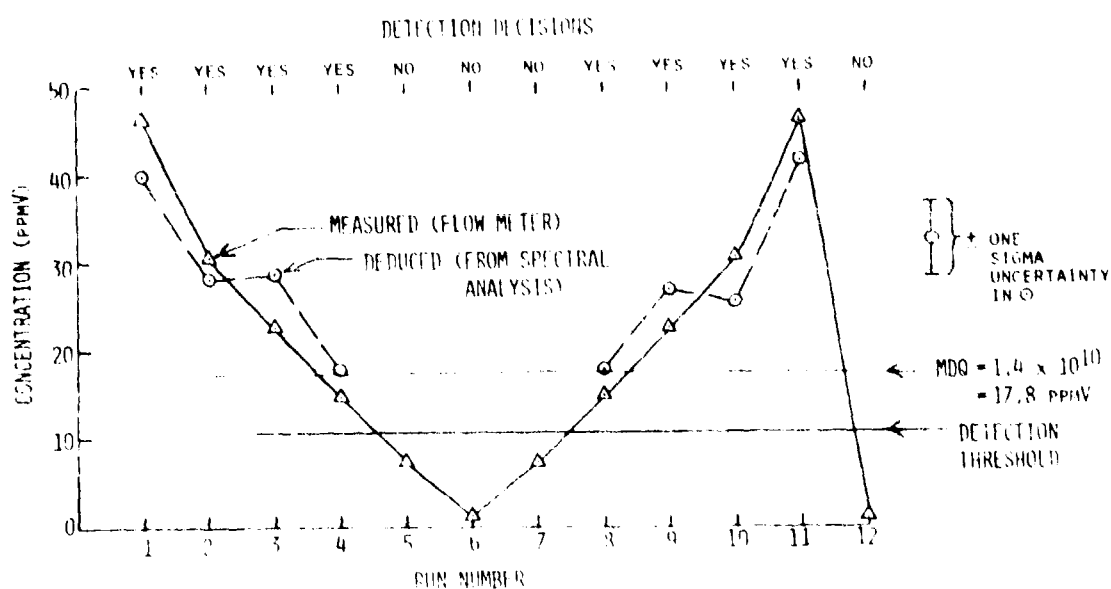
Figure 2. Comparison of analysis results and measured values for test of 19 February 1981

---

[*] The estimate of theoretical uncertainty may be high, since it is proportional to the system NESR, which was estimated from the difference between successive background spectra. That is, temporal background variations may have caused the uncertainty to be overestimated. This may explain the near-symmetry (approximate repeatability) of the deduced concentrations. It is possible that the deduced concentrations are more accurate than the measured values.

5

Figure 3 shows a computed reference contrast spectrum for one of the data runs, and two examples of measured contrast spectra that resulted in N_2O detection.[*] The middle panel of the figure shows the measured contrast when the detectable amount is approximately four times the MDQ. At this level the presence of N_2O is barely discernible by visual examination of the spectrum. In the bottom panel the detectable amount is ~1.5 times the MDQ. There is extremely high probability of detection (~~ 0.95) when the detectable amount is 1.5 times the MDQ, even though the measured contrast spectrum for this amount looks like noise. The spectrum signal-to-noise is only 0.26 for the bottom panel in Fig. 3; at the MDQ level the S/N would be 0.15. The "flat spots" between 2250 and 2260 cm^{-1} in the two measured contrast spectra represent spectral elements that were excluded in the correlation detection processing. The excluded elements have very low atmospheric transmittance (hence, little information) due to the very strong isotopic CO_2 lines seen in the top panel of the figure.

1.2 Conclusions

Analysis of the field test data revealed some unanticipated problems both with the data analysis methods and the FTS instrumentation. There was sufficient time remaining in the program after these problems were resolved to obtain valid data and to perform valid analyses of the data. The identification and solution of the problems, which are discussed in Sections 3 and 4, was a useful byproduct of the program.

The major conclusions of the study are:

(1) The concept has been validated completely by computer simulation. The simulation verified the predicted detection probability, false detection probability, and uncertainty in the detected quantity at levels equal to and lower than the MDQ level. The simulations used a field-measured contrast spectrum, and computer-generated noise.

(2) Detectable amounts obtained by spectral analysis of the field data taken in January and February are in excellent agreement with

---

[*] Actually $-\Delta N_\nu = N_1 - N_2$ is shown. ΔN_ν is negative because N_2O was observed in absorption rather than emission.
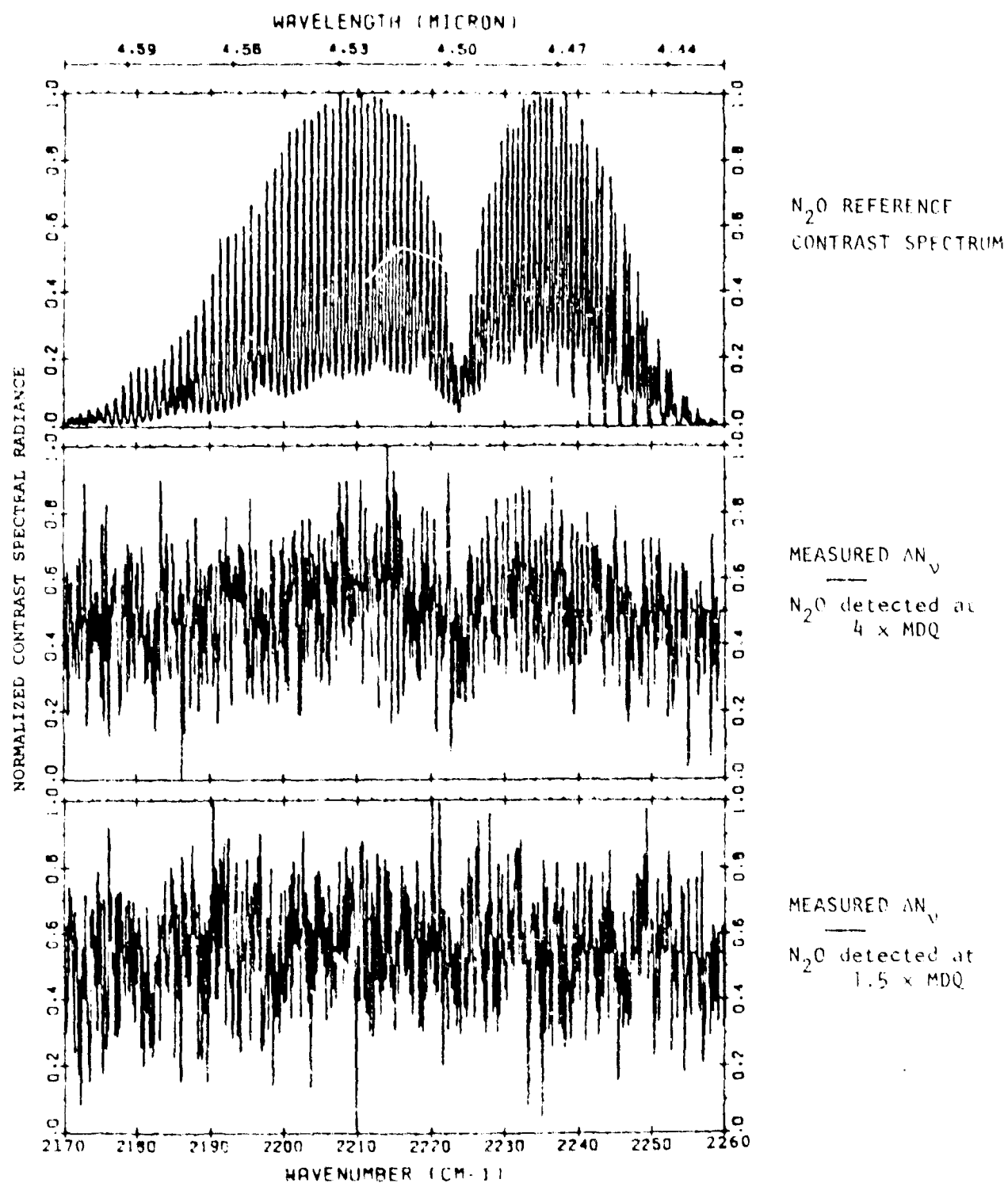
Figure 3. Normalized reference contrast spectrum for ν_3 band of N_2O (top panel) and two normalized contrast spectra obtained from measurements.

directly measured amounts. The quantity of field data obtained was not sufficient to allow estimation of actual detection and false detection probabilities.

(3) The calculated MDQ's and thresholds are possibly too high, as a result of unknown background temperature variations. This means only that we may have underestimated the detection capabilities of the USU FTS field system; the possible error in MDQ does not affect the inferred amounts.

(4) We examined the possibility of inferring the target gas column thickness and temperature and the background temperature by a more detailed analysis of the measured spectra, and have concluded that these quantities can be determined with reasonable accuracy when the detectable quantity is much greater than the MDQ. However, if the target cloud contains another species (such as CO_2) that may not be of particular interest but is present in sufficiently large quantity, the cloud temperature can be determined with high accuracy by a detailed analysis of its spectrum, and then the target gas column thickness can be inferred with high accuracy, even if the target gas is present at the MDQ level. The capabilities of the method to infer target gas column thickness and temperature requires a detailed specification of the expected total composition of the cloud.

SECTION 2
REVIEW OF THEORY

The idea of a minimum detectable quantity implies low target gas concentrations. It also implies a benign background, since background (and atmospheric) interferences would generally require using a higher detection threshold, which would allow detection only at higher concentration levels. Specifically, it will be assumed that the target cloud is optically thin in the spectral bands used for detection, and that the background and atmosphere in the two fields of view (IFOV's) used to obtain the spectral contrast are identical. The only type of interference included in this section is system (detector) noise. The effects of some types of atmospheric and background interferences are analyzed in Ref. 1.

Under the stated assumptions the spectral radiance contrast for the two IFOV's indicated in Fig. 1 is given by[1]

$$\Delta N_\nu \equiv N_2 - N_1 \simeq D\tau_\nu \alpha_{g\nu}; \quad D = u\overline{\Delta B}_\nu (T_g, T_{sfc}) \tag{1}$$

where

τ_ν = atmospheric spectral transmittance between the target and sensor,

$\alpha_{g\nu}$ = spectral absorption coefficient of the (single) target gas,

u = molecular column thickness of the target gas (number of molecules per unit area in the line-of-sight),

and $\overline{\Delta B}_\nu$ = difference between the spectral radiance of a blackbody at the gas temperature T_g and the actual spectral radiance of the background at temperature T_{sfc}, averaged over the detection spectral band.

The detectable quantity, denoted by D, is essentially a scale factor in the measured contrast spectrum. Equation (1) is an approximation only because we have replaced the actual spectral variation ΔB_ν by its average value. However, the variation is slow compared to that of τ_ν and $\alpha_{g\nu}$ and is nearly linear over narrow detection bands, so that the approximation is a good one,

9

especially if $\tau_\nu \simeq 1$ and $\alpha_{g\nu}$ is more-or-less symmetrical about the center of the detection band.

A reasonably accurate theoretical estimate of $\tau_\nu \alpha_{g\nu}$ can be obtained using a line-by-line computer code such as AFGL's FASCOD1.[6] Then an estimate D' of D can be obtained by finding the value that minimizes the mean square difference between the measured spectrum ΔN_ν and $D'\tau_\nu \alpha_{g\nu}$. Of course, $\alpha_{g\nu}$ is a function of the gas temperature, but $\partial \ln \alpha_{g\nu}/\partial T_g \ll \partial \ln \Delta B_\nu/\partial T_g$. Hence, the use of some guess temperature in computing $\alpha_{g\nu}$ will not result in a large error in D'.

Some simple types of background and atmospheric interferences can be suppressed by subtracting the means of ΔN_ν and $\tau_\nu \alpha_{g\nu}$ from these spectra before they are used to estimate D. The least-squares estimator of D is then[1]

$$D' = \frac{\sum (a-\bar{a})(b-\bar{b})}{\sum (b-\bar{b})^2} \equiv \frac{\sigma_{ab}}{\sigma_b^2} \tag{2}$$

where $a \equiv \Delta N_\nu + NOISE_\nu$, $b \equiv \tau_\nu \alpha_{g\nu}$, and the summations are over the digitized spectrum values. Equation (2) is the prescription for computing the estimate D' given the measurement a and *reference contrast spectrum* b. By combining Eqs. (1) and (2), we find that D' can also be expressed by

$$D' = D + \frac{\sigma_{bn}}{\sigma_b^2} \tag{3}$$

where σ_{bn} is the covariance of the digitized reference spectrum and the spectrum noise, and σ_b^2 is the variance of the digitized reference spectrum.

The spectrum noise samples will be Gaussian with zero mean, and the samples will also be independent provided the sample spacing is not smaller than the resolution $\Delta \nu$ of the FTS system. It can be shown[1] that if the spacing is $\Delta \nu$ the second term of Eq. (3) is

$$\frac{\sigma_{bn}}{\sigma_b^2} = \frac{x\sigma_n}{\sqrt{M}\,\sigma_b} = x\,\frac{\sqrt{2}\,\overline{NESR}}{\sqrt{M}\,\sigma_b} \equiv x\sigma_{D'} \tag{4}$$

where x is a unit normal random variate, M is the total number of resolved spectral elements in the spectra a and b, and $\overline{NESR}$ is the average system noise-equivalent spectral radiance over the detection band. Note that the effective rms noise σ_n equals $\sqrt{2}\,\overline{NESR}$ because ΔN_ν is the difference of two measurements with independent noise. Thus, the rms uncertainty in D' is $\sigma_{D'} \equiv \sqrt{2}\,\overline{NESR}/(\sqrt{M}\,\sigma_b)$.

The quantity

$$\frac{\sigma_b D}{\sqrt{2}\,\overline{NESR}} \equiv \text{"}\frac{S}{N}\text{"} \tag{5}$$

is the rms signal variation [from Eq. (1) and the definition of σ_b] divided by the rms spectral noise; i.e., it is the spectral *detection signal-to-noise*. Since $D'/\sigma_{D'}$ is this quantity times $\sqrt{M}$, it is evident that for sufficiently large M the detectable quantity can be estimated accurately even if local spectrum features are well below the noise level ($S/N \ll 1$).

D will be negative if the target gas is observed in absorption (is "cooler" than the background) and positive if it is observed in emission. Hence, detection of the target gas can be based on the test

$$|D'| \overset{?}{\underset{>}{}} R_D \tag{6}$$

where R_D is some predetermined threshold. Knowing the statistics of D' (Eqs. 3 and 4) we can work out the statistics for $|D'|$ for both target present ($D \neq 0$) and target not present ($D = 0$), and finally determine a threshold R_D that yields satisfactory detection and false detection probabilities.

Equations (3) and (4) show that the probability density function (p.d.f.) of D' is normal with mean D and standard deviation $\sigma_{D'} = \sqrt{2}\,\overline{NESR}/(\sqrt{M}\,\sigma_b)$. The p.f.d. has zero mean if the target is not present. It is well known that the p.d.f. of the absolute value of a random variate x is

$$g_1(|x|) = g(x) + g(-x) \tag{7}$$

if $g(x)$ denotes the p.d.f. of x. Hence, $|D´|$ has the p.d.f. indicated by Fig. 4 (and the upper abscissa scale). That is, the p.d.f.'s of $|D´|$ for $D = 0$ and $D \neq 0$ are 2 x normal and approximately normal, respectively, provided we can assume that the original p.d.f. of $D´$ for $D \neq 0$ has essentially no overlap with its mirror image [$g(-x) \simeq 0$ everywhere that $g(x)$'s appreciably different from zero]. This assumption will always be valid if the resulting p.d.f.'s can yield high system performance, e.g., detection probability equal to 95 percent and false detection probability equal to one percent.
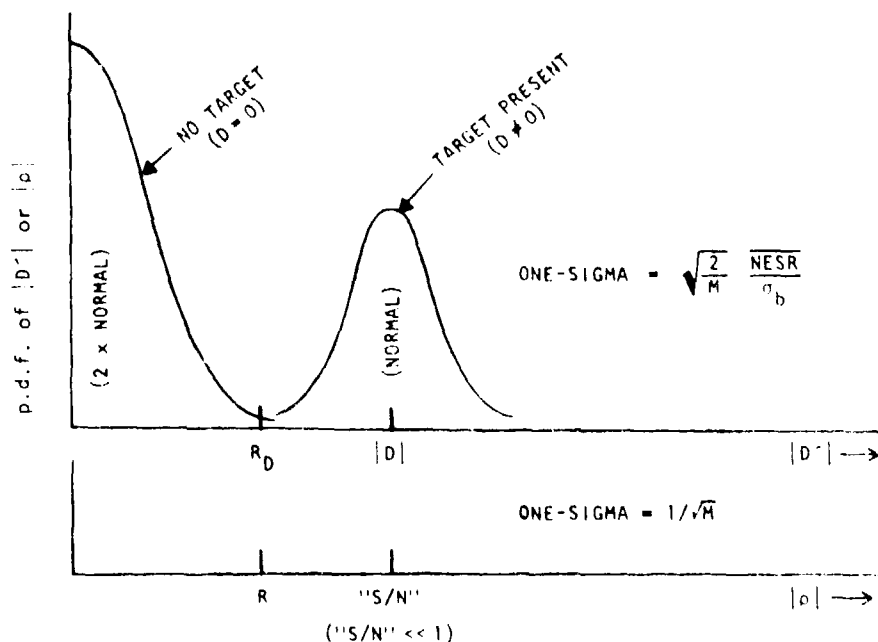

Figure 4. The probability density functions for $|D´|$ and $|\rho|$. These are valid for $|\rho|$ provided "S/N" << 1.

The detection probability $P(T|T)$ and false detection probability $P(T|0)$ are defined by

$$P(T|T) = \int_{R_D}^{\infty} \text{p.d.f.} \ (D \neq 0) \ d|D´|$$

$$\text{and} \quad P(T|0) = \int_{R_D}^{\infty} \text{p.d.f.} \ (D = 0) \ d|D´| \ . \tag{8}$$

12

se probabilities are the areas under the two curves in Fig. 4 at $|D'| > R_D$. It is evident that $P(T|T)$ depends on R_D, σ_D, and D, and that $P(T|0)$ depends on R_D and σ_D, only. Standard tables of the normal distribution (integrals of a unit normal p.d.f.) can be used to show that the threshold value

$$R_D = 2.58 \, \sigma_{D'} = 2.58 \frac{\sqrt{2} \, \overline{NESR}}{\sqrt{M} \, \sigma_b} \tag{9}$$

results in approximately 95 percent detection probability and approximately one percent false detection probability when D equals

$$4.23 \, \sigma_{D'} = 4.23 \frac{\sqrt{2} \, \overline{NESR}}{\sqrt{M} \, \sigma_b} \equiv MDQ \, . \tag{10}$$

This, by definition, is the minimum detectable quantity. Note that $R_D = 0.610 \times MDQ$.

The $\overline{NESR}$, M and σ_b all vary with the spectrometer resolution $\Delta\nu$. One can show that a near-optimum value for $\Delta\nu$ is the halfwidth of the target gas spectral lines, which is $\sim 0.1 \ cm^{-1}$ for targets near sea-level. That is, $\Delta\nu \simeq 0.1 \ cm^{-1}$ will give the smallest MDQ from Eq. (10).[*] The single parameter in Eq. (10) that depends on the target gas and detection geometry is σ_b, the standard deviation of the reference spectrum $\tau_\nu \alpha_{g\nu}$ degraded to $0.1 \ cm^{-1}$ resolution.

2.1 Statistics of the Correlation Coefficient

In the previous study[1] a numerical procedure was developed for computing the statistics of the spectral correlation coefficient ρ, defined by

$$\rho \equiv \frac{\sum (a-\overline{a})(b-\overline{b})}{\left\{ \left[\sum (a-\overline{a})^2 \right] \left[\sum (b-\overline{b})^2 \right] \right\}^{1/2}} \equiv \frac{\sigma_{ab}}{\sigma_a \sigma_b} \, . \tag{11}$$

---

[*] One can use spectra having many points per $\Delta\nu$ -- this would not appreciably affect the MDQ, but Eq. (10) would not be valid for calculating the MDQ unless M is redefined. Equations (4), (9) and (10) are valid only if the M noise samples are independent.

The test for detection proposed in Ref. 1 was

$$|\rho| \overset{?}{>} R \, . \tag{12}$$

We will show that this test is equivalent to $|D'| \overset{?}{>} R_D$ (Eq. 6) provided $S/N \ll 1$.

Comparison of Eqs. (2) and (11) shows that

$$\rho = (\sigma_b/\sigma_a)D' \, . \tag{13}$$

Substituting Eqs. (3) and (4), which define D', into (13), we obtain

$$\rho = \frac{\sigma_b}{\sigma_a} D + \frac{x}{\sqrt{M}} \frac{\sigma_n}{\sigma_a} \tag{14}$$

where x is again a unit normal random variate. We recall that $a \equiv \Delta N_\nu + NOISE_\nu$; hence ρ does not have a simple (normal) p.d.f., like D'. However, *in the case of very low S/N*, $\sigma_a \simeq \sigma_n$, and

$$\rho \simeq \frac{\sigma_b}{\sigma_n} D' = \frac{\sigma_b}{\sigma_n} D + \frac{x}{\sqrt{M}}$$

$$= \frac{"S"}{N} + \frac{x}{\sqrt{M}} \tag{15}$$

This result means that if S/N is very low, the random variate $|\rho|$ and $|(\sigma_b/\sigma_n)D'|$ have the same p.d.f.'s, as indicated by the two abscissa scales in Fig. 4. In particular, the test (12), with

$$R = \frac{\sigma_b}{\sigma_n} R_D = \frac{2.58}{\sqrt{M}} \tag{16}$$

will also give $P(T|T) = 0.95$ and $P(T|0) = 0.01$ when $D = MDQ$. Since $S/N \ll 1$ when D is near the MDQ level for the N_2O detection band used in the field

tests (and for all detection bands analyzed in Ref. 1), the tests (6) and (12) will give the same results.[*]

The correlation coefficient would be a better detection parameter than D' when S/N is large and there are spectral interferences corresponding to very large S/N.

2.2 Calculation of $P(T|T)$ and $P(T|0)$

If $D \neq MDQ$ and/or the threshold (R or R_D) is not set to the value given by Eq. (9) or (16), the detection and false detection probabilities can be different from 0.95 and 0.01. If detection is based on the correlation coefficient ρ (and if S/N << 1), the general equations are

$$P(T|T) = \int_{-\infty}^{p} g(x)\, dx \tag{17}$$

$$P(T|0) = 2 \int_{q}^{\infty} g(x)\, dx\ , \tag{18}$$

where $g(x) = (1/\sqrt{2\pi})\exp(-x^2/2)$ is the unit normal density function and

$$p = [f \cdot (''S/N'') - R]\ \sqrt{M} \tag{19}$$

$$q = R\ \sqrt{M}\ . \tag{20}$$

The ratio ''S/N'' (which was denoted Z in Ref. 1) is given by Eq. (5). The parameter $f \leq 1$ is defined as the correlation coefficient between the reference spectrum and a *very high S/N* measured contrast spectrum. Generally, a value less than unity indicates that the reference spectrum is not perfect and/or that the spectrometer system is not perfectly calibrated. Note that $P(T|T)$ will be less than 0.95 if $f < 1$, even if $D = MDQ$ and R is given by Eq. (16). The integrals in (17) and (18) are tabulated in mathematical reference books.

---

[*]The MDQ's given in Ref. 1 are correct. Approximate values could have been calculated from standard tables of the normal distribution, rather than the numerical procedure defined in Ref. 1.

If detection is based on the estimate D' of D (Eq. 6), the above equations for $P(T|.)$ and $P(T|0)$ are valid, provided p and q are redefined:

$$p \rightarrow p' = [f \cdot |D| - R_D]/\sigma_{D'} . \tag{21}$$

$$\sigma_{D'} = \sqrt{2} \ \overline{NESR}/(\sqrt{M} \ \sigma_b) , \tag{22}$$

$$q \rightarrow q' = R_D/\sigma_{D'} . \tag{23}$$

The detectable amounts D' in unit of $(molecules/cm^2)(W/cm^2\text{-}sr\text{-}cm^{-1})$ can be converted to volume concentration C in ppmV from the formula

$$C = \frac{D'}{\overline{\Delta B}_\nu} \ \frac{10^6}{2.69 \times 10^{19}} \ \frac{T_g(k)}{273} \ \frac{1013}{p_g(mb)} \ \frac{1}{L(m)}$$

where p_g is the gas (ambient) pressure and L is the path length through the gas.

SECTION 3
COMPUTER SIMULATION

The equations for predicting system performance are based on the assumption that the system spectral noise is Gaussian (and white). It was felt that this assumption should be tested before performing the computer simulation and field data analyses.

USU provided noise spectra obtained by differencing spectral measurements of a blackbody. The FTS system observed the blackbody at very close range t minimize any effects of time-varying atmospheric absorption. ARC used the standard chi-square test for goodness-of-fit to test the hypothesis that the spectrum noise samples obey a normal distribution. The data samples were spaced approximately 0.06 cm^{-1} apart and the FTS resolution (full width at half maximum) was approximately 0.132 cm^{-1}. Alternate samples were discarded in the tests, so that the noise samples had an effective spacing of ~0.12 cm^{-1} and could be considered uncorrelated.

Initially, the entire noise spectrum from 2170 cm^{-1} to 2260 cm^{-1} was used. The first series of tests involved 21 spectra, each consisting of 747 usable samples. The chi-square test with four degrees of freedom and a significance level of five percent was applied to each spectrum individually. All 21 tests failed, and by a large margin.

Figure 5 shows why the tests failed: The noise spectrum obviously is not white, and as a result, the set of noise samples is non-normal. The spectral noise is not white because it has been calibrated; i.e., the noise voltage has been divided by the spectral responsivity of the FTS system. The calibrated noise is large near the edges of the detection band because the system includes a cooled circular variable filter (CVF) which has low transmission near the band edges. The purpose of the CVF is, of course, to reduce the total photon flux on the detector; i.e., to minimize the system $\overline{NESR}$.
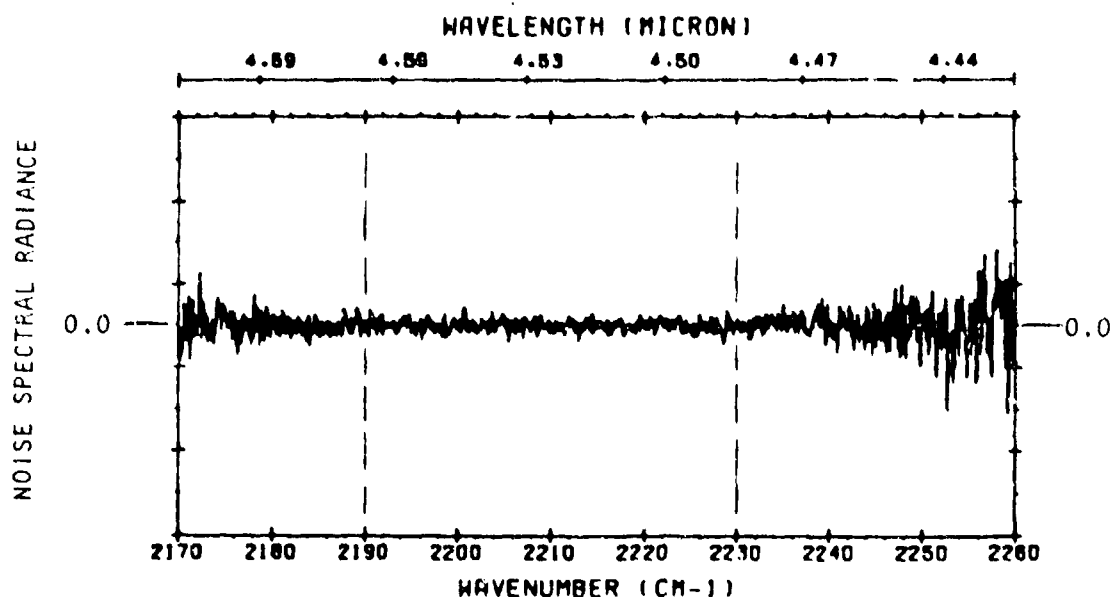
17

Figure 5. Example of a (calibrated) system noise spectrum obtained
by differencing two measured spectra of a blackbody.

The noise should be white if it is not calibrated. In fact, we realized
from these initial tests that it would be best to base detection on the
analysis of *uncalibrated* spectral data. The FTS spectral responsivity func-
tion should be applied instead to the reference contrast spectrum; i.e., the
reference spectrum should be *multiplied* by the spectral responsivity. Then
detection would be based on the correlation of two spectra with units of volts
rather than spectral radiance units. The multiplicative calibration procedure
was used in the analyses of field data reported in Section 4.

Rather than attempt to "uncalibrate" the available noise spectra, we
narrowed the spectral region to 2190-2230 cm^{-1}, over which the noise is
approximately white (see Fig. 5). Some of the noise spectra had a non-zero
spectrally varying average value, indicating that the system spectral respon-
sivity had varied during or between the pair of blackbody spectral measurements.
Noise spectra having this behavior in the narrowed spectral region were
discarded. Twenty-six spectra of 333 samples each were individually subjected
to a pair of chi-square tests:

TEST A: Two degrees of freedom, significance level five percent

TEST B: Two degrees of freedom, significance level one percent

18

It was necessary to decrease the number of degrees of freedom from four to two because of the reduced sample size. Twenty-three of the 26 spectra passed Test A. All of the spectra passed Test B. It is concluded that the noise is normal (and white) over the region of uniform spectral response, and is also normal (and white) over the entire 2170-2260 cm^{-1} detection band if the measurements are not calibrated.

The remainder of this section describes a computer simulation that validated the performance statistics predicted by the model described in Section 2. It was recognized that while the field tests might provide an impressive real-world demonstration of the method, their number would not be sufficient to compile meaningful statistics. It was practical to simulate several thousand tests on the computer whereas the planned number o field tests was only 100.

The simulation consisted of repeatedly adding computer-generated noise to a high-S/N contrast spectrum measured by USU. This resulted in an artificial data base that could be analyzed in the same way as real data. We first analyzed the high-S/N contrast spectrum to estimate the detectable quantity D (from Eq. 2). Knowing the rms spectral signal $\sigma_a \simeq \sigma_b D$ to high accuracy, we could adjust the rms value σ_n of the added noise to obtain a particular value of signal-to-noise, "S/N" = $(\sigma_b D/\sigma_n)$ (Eq. 5). For various choices of "S/N" and threshold R, we could forecast the detection and false detection probabilities (Eqs. 17 through 20). The "data" was analyzed (according to Eqs. 11 and 12), and the fraction of successful detections was compared to the forecast detection probability. The computer-generated noise was analyzed in the same way to obtain a comparison of actual and forecast false detection probabilities.

Figure 6 shows the high-S/N measured contrast spectrum on a normalized (0 to 1.0) scale. The spectrum is calibrated, and has been truncated to the spectral region ~2192-2252 cm^{-1}. The non-white character of the noise is not important since the S/N is reduced considerably in the simulation. The effective sample spacing is ~0.12 cm^{-1} and the effective number of samples M is 500.[*]

---

[*] All spectrum plots in this report, however, show computed or measured spectra at ~0.132 cm^{-1} resolution, with points spaced at 0.06 cm^{-1}.
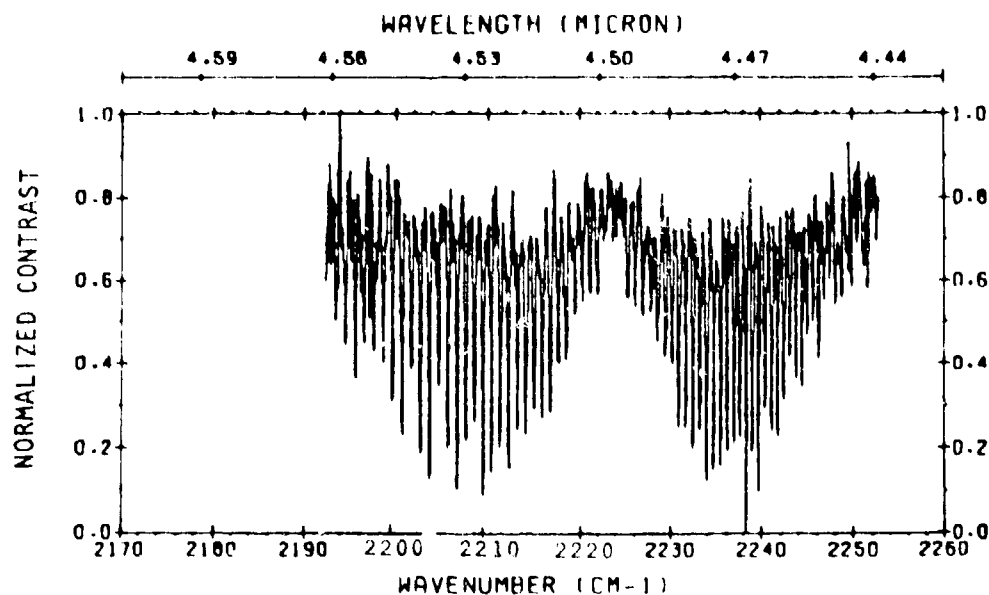
WAVELENGTH (MICRON)

NORMALIZED CONTRAST

WAVENUMBER (CM-1)

Figure 6.   Truncated USU high-S/N contrast spectrum used in computer simulation (spectral range $\simeq$ 2192-2252 cm^{-1})

It was determined that the high-S/N measured contrast spectrum was not perfectly correlated with the reference spectrum: the correlation coefficient was 0.902.   This value of f was used in Eq. (19) to calculate the predicted detection probability.

The reference spectrum was computed using AFGL's FASCOD1 computer code[6] and meteorological data supplied by USU.   The instrument spectral line shape (ILS) corresponding to the interferogram apodization used by USU is called the Happ-Genzel line shape.[7]   It was necessary to incorporate this particular ILS into one of FASCOD1's subroutines.

The results of the simulation are shown in Table 1.   The four cases represent selected combinations of "S/N" and threshold R which correspond to a wide range of predicted detection and false detection probabilities.   The actual probabilities are based on analysis of 1,000 signal-plus-noise spectra. The table gives two values for each case because the analysis was performed twice for independent noise sets.   The table includes a comparison of predicted and actual relative uncertainty in the inferred detectable quantity, σ_D/D [The predicted value of σ_D/D is $(1/\sqrt{M})("N/S")$, from Eqs. (4) and (5)].

20

Table 1. Results of Computer Simulation

CASE	"S/N"	R	$P(T|T)$ Predicted	Actuals	$P(T'|0)$ Predicted	Actuals	σ_D/D Predicted	Actuals
1	0.17	0.10	0.88	0.84, 0.84	0.025	0.022, 0.024	0.180	0.181, 0.173
2	0.15	0.14	0.46	0.36, 0.39	0.0018	0.0030, 0.0040	0.204	0.205, 0.197
3	0.11	0.05	0.86	0.84, 0.84	0.26	0.25, 0.26	0.278	0.280, 0.268
4	0.11	0.12	0.32	0.26, 0.28	0.0074	0.012, 0.0080	0.278	0.280, 0.268

Estimate of D from high-S/N data $= -2.98 \times 10^{10} (\text{molec/cm}^2)(\text{W/cm}^2\text{-sr-cm}^{-1})$

21

As the table shows, there is excellent agreement between the actual and predicted values, except when the predicted $P(T|0)$ is much less than one percent (Case 2). There is particularly good agreement for the first case, which is closest to the MDQ performance level.

Note that we have really tested the method at a level very close to the MDQ, for if the high-S/N USU contrast spectrum and reference spectrum were perfectly correlated ($f = 1$ rather than 0.902 in Eq. (19)), the predicted $P(T|T)$ for the first case could be 0.94 rather than 0.88. The actual $P(T|T)$ would also be higher, and in good agreement with the prediction. In the actual practice of the detection method, "perfect" reference spectra could be obtained from high S/N laboratory measurements using the actual FTS detection system; i.e., determination of the reference spectrum could be part of the system calibration procedure.

SECTION 4
ANALYSIS OF FIELD MEASUREMENTS

The problem of time-varying spectral responsivity referred to in the previous section was encountered again during analysis of the low-S/N field measurements. When no target N_2O is present the contrast radiance spectrum should be just noise, but if the spectral responsivity has changed between the two measurements, their difference (the spectral contrast) will contain an additional component with a slow spectral variation. This component will result in a false detection if it is comparable to the signal level $\sigma_b D$ and if it resembles even slightly the band contour of the reference spectrum. Similarly, the varying responsivity can result in missed detections and/or large errors in the inferred detectable quantity when the target N_2O is present. These effects were observed in the analysis of the first several sets of field data.

The remedy was simple. USU modified the FTS system to bypass the cooled CVF in the optical train, and the problem disappeared.

Estimates of the effective rms system noise $\sigma_n \equiv \sqrt{2} \; \overline{NESR}$ were needed to set the detection threshold, to estimate the MDQ, and to determine the expected uncertainty in the inferred detectable amounts. A single estimate was obtained for each series of runs by computing the average of the rms uncalibrated spectral radiance difference between consecutive pairs of background runs. For each series, the value of σ_n thus obtained was approximately 1.2 mV. Figure 7 shows individual σ_n values determined from consecutive background spectrum pairs for five series of runs made in January and February 1981. The fact that the variation in σ_n over a series of runs slightly exceeds the 95 percent confidence limits on this estimate indicates that the background temperature and/or FTS responsivity may have varied slightly during a series. However, the variations are extremely small compared to those observed when the CVF was used in the system.
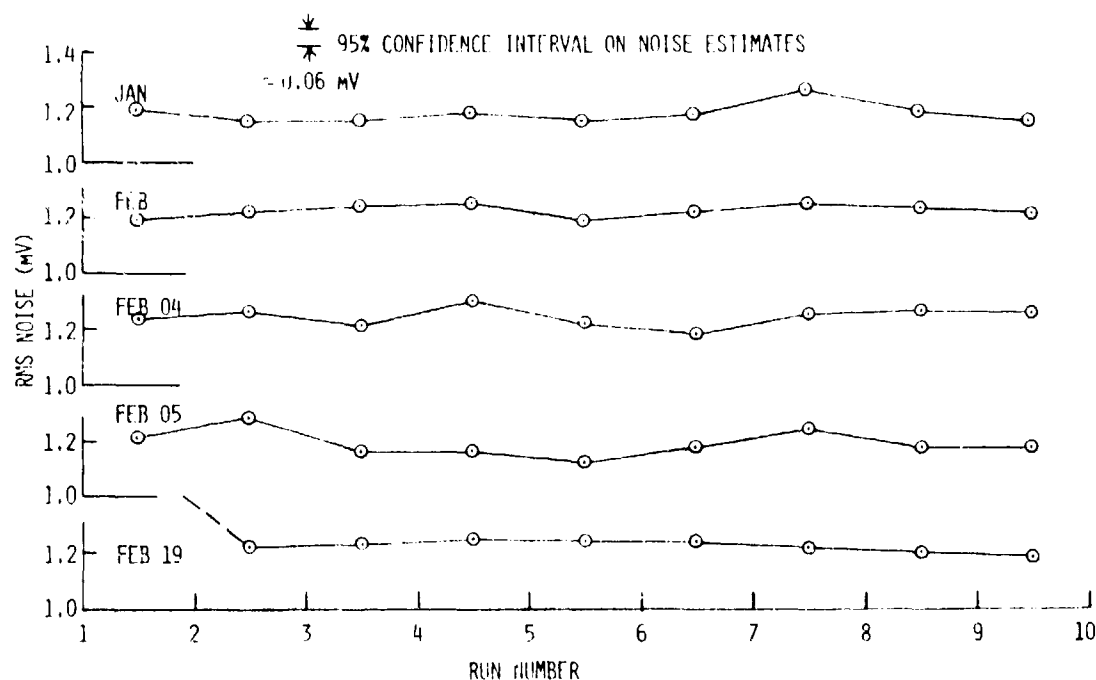
23

Figure 7. Noise estimates from differences of successive background runs

A typical N_2O reference contrast spectrum was shown earlier (Fig. 3). For the January and February series of field tests the standard deviation σ_b of the computed reference spectrum varied between 1.33×10^{-14} and 1.4×10^{-14} $(cm^2/molec)(volts/W/cm^2-sr-cm^{-1})$.

Figure 8 shows a typical FASCOD1 computed transmittance spectrum for the USU 273-meter path. The major absorptions are by atmospheric N_2O and $C^{13}O_2^{16}$. The transmittance spectrum τ_ν is included in the "calibrated" reference spectrum $\tau_\nu \alpha_{g\nu} R_\nu$, where R_ν is the system spectral responsivity. Spectral elements with $\tau_\nu < 0.1$ were excluded from the detection processing. For the January and February tests the effective number of spectral elements M was between 709 and 813.

Figure 9 is a typical radiance spectrum computed for the USU 273-meter path. The figure gives an indication of how the measured target and background spectra would look if they were calibrated.

Tables A-1 through A-5 in Appendix A reproduce the computer printouts of the data analysis results for the January and February field tests. These results are summarized in Table 2. The second column of the table gives the

24

WAVELENGTH (MICRON)

4.59   4.56   4.53   4.50   4.47   4.44
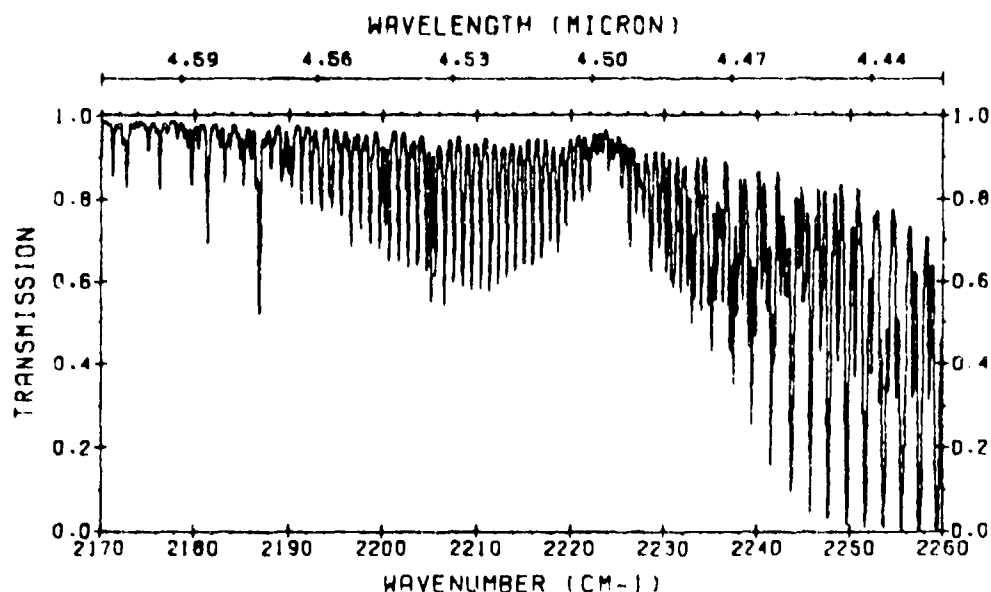
Figure 8. Typical FASCOD1 computed spectral transmission
for the USU 273-meter path

WAVELENGTH (MICRON)

4.59   4.56   4.53   4.50   4.47   4.44
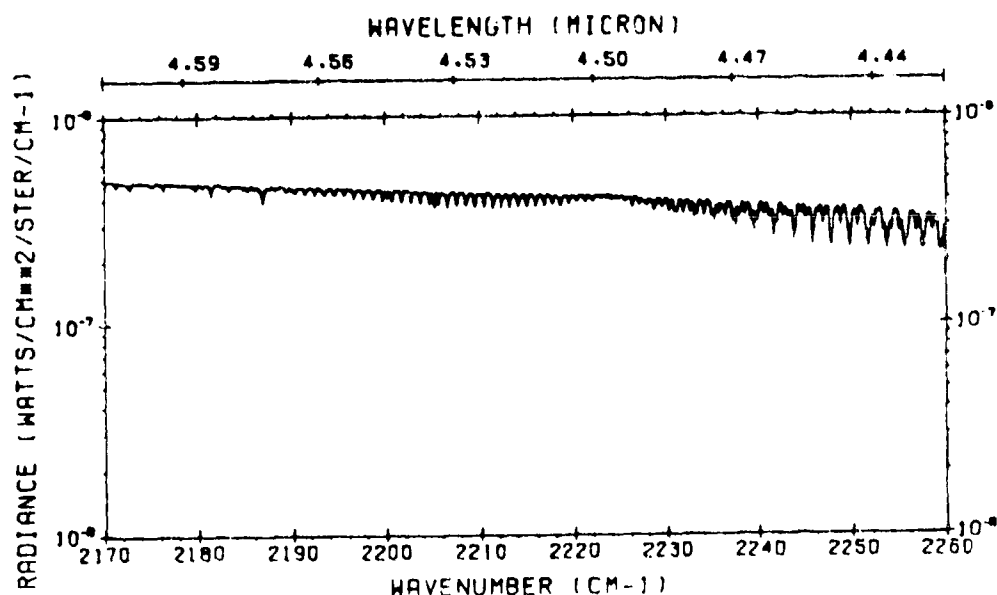
Figure 9. Typical FASCOD1 computed spectral radiance for
the USU 273-meter path

number of detections, and the third the computed MDQ. The remaining columns
give the average of the inferred detectable quantity for the series of 12
runs, the standard deviation of these estimates, and the predicted standard
deviation, all normalized to the MDQ. The results of the 19 February test,

25

Table 2. Summary of Detection Results for January and February 1981 Data Sets

DATA SET	NO. OF DETECTIONS	MDQ	AVG D´/MDQ	$\sigma_{D´}$/MDQ	PREDICTED $\sigma_{D´}$/MDQ
JAN	12 (ALL)	1.36×10^{10}	1.66	0.30	0.24
FEB	12 (ALL)	1.37×10^{10}	3.88	0.64	0.24
FEB 04	12 (ALL)	1.48×10^{10}	1.72	0.32	0.24
FEB 05	12 (ALL)	1.39×10^{10}	2.14	0.30	0.24
FEB 19*	8	1.40×10^{10}	(N.A.)	(N.A.)	(0.24)

*Flow rate purposely varied.

DATA SET	INFERRED AVG CONC (ppmV)	MEASURED AVG CONC (ppmV)
FEB	54 ± 13	40
FEB 05	30.4 ± 7.3	35.9
FEB 19	(SEE FIGURE 2)	

in which the flow rate was purposely varied, was already described in Section I. The second part of the table compares the average D' converted to N_2O concentration and the measured concentration for two of the field tests.

It is seen that the agreement between inferred and measured concentrations is essentially within the calculated $\pm$ one-sigma uncertainty in the inferences. Also, the actual relative standard deviations agree well with the estimated value, except for the "February" data set. The small differences (0.3 compared to 0.24) are probably due to background variations or very small responsivity changes.

SECTION 5

ESTIMATION OF GAS TEMPERATURE AND COLUMN THICKNESS

The temperature T_{sfc} of the background, if it is assumed to radiate as greybody or blackbody, can be estimated by careful analysis of the measured background spectrum and/or target-plus-background spectrum. Depending on the target species, it may be desirable to use a spectral region different from the detection band, i.e., an atmospheric window for which $\tau_\nu \simeq 1$ in many or all spectral elements. Once T_{sfc} is known, the target gas temperature T_g and column thickness u can be estimated by a more detailed analysis of spectra measured in the detection band.

Let a_ν denote ΔN_ν + $NOISE_\nu$ and b_ν a reference contrast spectrum. If it is desirable to subtract the average values of these two contrast spectra before correlation (e.g., if the background is known to have large spatial or temporal variations on the scale of the IFOV separation and spectrum measurement time), let a_ν and b_ν be defined as the remainders. Since T_g is to be inferred it is appropriate to redefine the reference contrast spectrum b_ν to include all dependences on T_g:

$$b_\nu = \tau_\nu \alpha_{g\nu} \longrightarrow \tau_\nu \alpha_{g\nu}(T_g) \Delta B_\nu(T_g, T_{sfc}) . \qquad (24)$$

The new reference spectrum b_ν can be computed (as before, via FASCOD1) using a particular guess (T´) for T_g. The object is to obtain estimates u´ and T´ that minimize the rms error in the equation

$$a_\nu = u´ b_\nu(T´, T_{sfc}) , \qquad (25)$$

which is merely Eq. (1) written in different notation. The least squares minimization procedure for determining u´ and T´ is nonlinear, whereas the one for estimating D was linear (within the stated approximations).

By formally minimizing the mean-square difference between the right- and left-hand sides of Eq. (25) with respect to both u´ and T´, we obtain a pair of solutions for u´:

$$u' = \sum a_\nu b_\nu(T', T_{sfc}) \bigg/ \sum b_\nu^2(T', T_{sfc}) \qquad (26a)$$

$$u' = \left(\sum a_\nu \frac{\partial b_\nu}{\partial T'} \right) \bigg/ \left(\sum b_\nu \frac{\partial b_\nu}{\partial T'} \right) \qquad (26b)$$

These two prescriptions for obtaining u' can be evaluated for a systematically-varied guess T', until they give the same result. The resultant u' and T' are the least-squares best solutions for u and T_g.

The solution method described is quite straightforward. However, analytical estimation of the errors in the solutions due to system noise in a_ν involves some tedious algebra. We performed a simplified analysis that assumes small errors. We will present only the results of the analysis.

The rms relative error $\delta u/u$ in inferred column thickness u and the rms error δT_g in inferred target gas temperature T_g are given by

$$\frac{\delta u}{u} = \frac{1}{\sqrt{M} Z} \left\{ 1 + \left| \frac{\partial \ln \overline{\Delta B}}{\partial T_g} \right| \frac{1}{(2k)^{1/2}} \right\} \qquad (27)$$

$$\delta T_g = \frac{1}{\sqrt{M} Z} \frac{1}{(2k)^{1/2}} \ , \qquad (28)$$

where

$$Z = u\sigma_b / (\sqrt{2} \ \overline{NESR}) \ , \qquad (29)$$

$$k = \lim_{\Delta T \to 0} \frac{1 - \rho[b_\nu(T_g), b_\nu(T_g + \Delta T)]}{(\Delta T)^2} \ . \qquad (30)$$

The derivative in Eq. (27) is $\partial \ln \overline{\Delta B}_\nu(1, T_{sfc}) / \partial T$ evaluated at $T = T_g$. The rms value of b_ν (*new definition*) is denoted σ_b; hence Z is essentially the same as the "S/N", given by Eq. (5). The parameter k may be defined as the coefficient of the quadratic term in the Taylor expansion of 1-ρ, where ρ is the correlation coefficient of the reference spectra $b_\nu(T_g)$ and $b_\nu(T_g + \Delta T)$. Essentially, k is a measure of the sensitivity of the spectral contour (rotational line intensity distribution) of the target gas absorption band to a change in the gas temperature. Note that δT_g is small for large k.

30

It should be mentioned that the random variates u′ and T′, whose standard deviations are given by Eqs. (27) and (28), are partially correlated. That is, the uncertainty or "noise" in u′ is the sum of two partially correlated normal variates, one of which is proportional to the "noise" in T′.[*] Equation (27) is always an overestimate of the rms error $\delta u/u$ since it assumes perfect positive correlation between the components of u′.

Equations (27) and (28) were evaluated for conditions typical of the USU field tests. The values $T_g = 295K$ and $T_{sfc} = 309K$ were used, and it was assumed that N_2O is present at the MDQ level. It was also assumed that T_g is the same as the atmospheric temperature.[**] The calculations gave

$$\delta u/u \simeq 4.0$$

$$\delta T_g \simeq 63K$$

(31)

which are absurdly large errors. Also, they are probably not accurate error estimates since Eqs. (27) and (28) were derived on the assumption of small errors. They show, however, that the errors would be of the order of $\delta u/u \simeq 0.4$ and $\delta T_g \simeq 6.3K$ if N_2O were present at ten times the MDQ level.[***]

These results confirmed our expectation that u and T_g cannot be determined accurately from the target gas contrast spectrum alone when the gas is present at the MDQ level. If some other "tracer" gas were present in such large quantity that T_g could be determined almost exactly from its spectrum, then the error $\delta u/u$ would be

$$\frac{\delta u}{u} \longrightarrow \frac{1}{\sqrt{M}\, Z}$$

(32)

which has the value 0.24 for N_2O at the MDQ level.

---

[*] Knowledge of the covariance matrix would be useful in defining a two-dimensional decision region that would maximize detection probability and minimize false detection probability. It would also allow accurate quantification of the errors δu and δT_g. We did not evaluate the correlation matrix because of the great amount of labor and computing time it would have required.

[**] And that it undergoes the same variation as the atmospheric temperature. This assumption effects the value of k calculated from Eq. (30).

[***] The error in δu is also strongly dependent on the temperature difference $|T_{sfc} - T_g|$.

REFERENCES

1. Zachor, A.S., "Down-Looking Interferometer Study," Vols. I & II, AFGL-TR-80-XXXX (To be published). Final Report on Utah State University Subcontract No. SC-79-012 (U.S. Air Force prime Contract No. F19628-77-C-0203) (1980).

2. Zachor, A.S., Bartschi, B. and DelGreco, F.P., "Minimum Detectable Quantities of Trace Gases using High-Resolution Spectroscopy," Proceedings of the 29th Symposium of the Electromagnetic Wave Propagation Panel of AGARD, Monterey, California, 6-10 April, 1981.

3. Zachor, A.S., Bartschi, B. and Ahmadjian, M., "Detection of Trace Gases using High-Resolution Spectroscopy," Proceedings of the SPIE Symposium on Atmospheric Transmission, Washington, D.C., 21-22 April, 1981 (SPIE Proceedings, Vol. 277).

4. Anapol, M., Titus, J., Corker, W. and Gunn, K., "Sensor Design Study," Space Systems Group, Inc., Final Report on Utah State University Subcontract No. SC-79-080 (U.S. Air Force prime Contract No. F19628-77-C-0203) (1979).

5. "Down-Looking Interferometer Study," Bartlett Systems, Inc., Report No. BSI-7711, Final Report on Utah State University P.O. No. 33349 (U.S. Air Force prime Contract No. F19628-74-C-0130) (1977).

6. Clough, S.A., Kneizys, F.X. and Rothman, L.S., "Atmospheric Spectral Transmittance and Radiance: FASCODE," Proceedings of the SPIE Symposium on Atmospheric Transmission, Washington, D.C., 21-22 April, 1981 (SPIE Proceedings, Vol. 277).

7. The Happ-Genzel line shape is the Fourier transform of the well-known Hamming window function. Its properties are described in Potter, R.W., Compilation of Time Windows and Line Shapes for Fourier Analysis," Hewlett Packard Company.

APPENDIX A

COMPUTER PRINTOUTS OF DATA ANALYSIS RESULTS

Table A.1 Data Analysis Results for Data Set JAN

CORRELATION RESULTS AND DETECTION DECISIONS FOR R= .0967

SET	AVGDN	SIGDN	COVAR	COEFF	DEC	D-EST
1	.7082E-03	.1713E-02	.5039E-17	.21868	YES	.2785E+11
2	.8700E-03	.1716E-02	.4366E-17	.18910	YES	.2413E+11
3	.6877E-03	.1616E-02	.3532E-17	.16251	YES	.1952E+11
4	.9724E-03	.1676E-02	.5254E-17	.23306	YES	.2904E+11
5	.3093E-03	.1756E-02	.4481E-17	.18969	YES	.2476E+11
6	.3931E-03	.1733E-02	.4039E-17	.17329	YES	.2233E+11
7	.7110E-03	.1640E-02	.4293E-17	.19462	YES	.2373E+11
8	.4340E-03	.1683E-02	.2986E-17	.13191	YES	.1650E+11
9	.7833E-03	.1695E-02	.4716E-17	.20683	YES	.2607E+11
10	.1245E-03	.1744E-02	.3194E-17	.13613	YES	.1765E+11
11	.6326E-03	.1679E-02	.4118E-17	.18230	YES	.2276E+11
12	.7673E-03	.1743E-02	.2979E-17	.12705	YES	.1646E+11

<meas ΔN_ν> (volts) — AVGDN column

s.t.d. of meas ΔN_ν (volts) — SIGDN column

covariance of ΔN_ν and reference spectrum — COVAR column

correlation coeff ρ — COEFF column

Decision — DEC column

D', the detectable quantity inferred from the data — D-EST column

Table A.2 Data Analysis Results for Data Set FEB

CORRELATION RESULTS AND DETECTION DECISIONS FOR R= .0967

SET	AVGON	SIGON	COVAR	COEFF	DEC	Q-EST
1	-.4190E-03	.1760E-02	-.5724E-17	-.24186	YES	-.3238E+11
2	-.1039E-02	.1902E-02	-.8574E-17	-.33798	YES	-.4851E+11
3	-.1050E-02	.1861E-02	-.1047E-16	-.42339	YES	-.5926E+11
4	-.1084E-02	.1865E-02	-.9538E-17	-.40081	YES	-.5622E+11
5	-.1214E-02	.1951E-02	-.1045E-16	-.40284	YES	-.5911E+11
6	-.1091E-02	.1916E-02	-.1007E-16	-.39528	YES	-.5656E+11
7	-.1224E-02	.1973E-02	-.8818E-17	-.33619	YES	-.4989E+11
8	-.1040E-02	.1842E-02	-.6944E-17	-.28351	YES	-.3929E+11
9	-.1181E-02	.1914E-02	-.9780E-17	-.38422	YES	-.5533E+11
10	-.1282E-02	.1926E-02	-.1015E-16	-.39591	YES	-.5740E+11
11	-.1105E-02	.1926E-02	-.1057E-16	-.41294	YES	-.5981E+11
12	-.1352E-02	.2040E-02	-.1137E-16	-.41698	YES	-.6430E+11

Table A.3 Data Analysis Results for Data Set FEB 04

CORRELATION RESULTS AND DETECTION DECISIONS FOR R = .0967

SET	AVGDN	SIGDN	COVAR	COEFF	DEC	D-EST
1	-.3217E-03	.1750E-02	-.6454E-17	-.27224	YES	-.3517E+11
2	-.3365E-03	.1802E-02	-.5731E-17	-.23473	YES	-.3122E+11
3	-.7261E-03	.1741E-02	-.4130E-17	-.17504	YES	-.2250E+11
4	-.5356E-03	.1726E-02	-.3723E-17	-.15927	YES	-.2029E+11
5	-.4406E-03	.1735E-02	-.3722E-17	-.15887	YES	-.2028E+11
6	-.5104E-03	.1724E-02	-.3847E-17	-.16469	YES	-.2096E+11
7	-.3264E-03	.1761E-02	-.3990E-17	-.16723	YES	-.2174E+11
8	-.3396E-03	.1787E-02	-.5165E-17	-.21338	YES	-.2814E+11
9	-.3788E-03	.1727E-02	-.5449E-17	-.23286	YES	-.2969E+11
10	-.6171E-03	.1855E-02	-.5274E-17	-.20989	YES	-.2873E+11
11	-.5912E-03	.1728E-02	-.3969E-17	-.16957	YES	-.2162E+11
12	-.5971E-03	.1745E-02	-.4624E-17	-.19564	YES	-.2519E+1_

Table A.4   Data Analysis Results for Data Set FEB 05

CORRELATION RESULTS AND DETECTION DECISIONS FOR R= .6967

SET	AVGON	SIGON	COVAR	COEFF	DEC	D-ST
1	-.0765E-03	.1777E-02	-.5663E-17	-.21427	YES	-.273 E+11
2	-.5679E-03	.1503E-02	-.4515E-17	-.21334	YES	-.2655E+11
3	-.3117E-03	.1724E-02	-.5086E-17	-.24253	YES	-.307 E+11
4	-.1203E-03	.1636E-02	-.6467E-17	-.21029	YES	-.3494E+11
5	-.4696E-03	.1660E-02	-.4762E-17	-.21092	YES	-.2573E+11
6	-.2011E-03	.1611E-02	-.5363E-17	-.23577	YES	-.265 E+11
7	-.3079E-03	.1704E-02	-.6735E-17	-.20561	YES	-.363 E+11
8	-.4136E-03	.1765E-02	-.5219E-17	-.22561	YES	-.292 E+11
9	-.3308E-03	.1606E-02	-.4071E-17	-.13629	YES	-.220 E+11
10	-.0609E-03	.1735E-02	-.6632E-17	-.23097	YES	-.358-E+11
11	-.2759E-03	.1747E-02	-.5904E-17	-.24562	YES	-.319 E+11
12	-.3238E-03	.1742E-02	-.5282E-17	-.22290	YES	-.265 E+11

Table A.5 Data Analysis Results for Data Set FEB 19

CORRELATION RESULTS AND DETECTION DECISIONS FOR R= .0269

SET	AVGCON	SIGCN	COVAR	COEFF	DEC	D-ST
1	-.36466E-03	.1904E-02	-.5940E-17	-.23931	YES	-.313 E+11
2	-.7059E-03	.1763E-02	-.4192E-17	-.17084	YES	-.2216E+11
3	-.3611E-03	.1822E-02	-.4291E-17	-.17112	YES	-.226 E+11
4	-.6338E-03	.1753E-02	-.2663E-17	-.11059	YES	-.140 E+11
5	-.6636E-03	.17-3E-02	-.402cE-18	-.02055	NO	
6	-.1409E-03	.1927E-02	-.1214E-17	-.00403	NO	
7	-.3392E-03	.1660E-02	-.1668E-17	-.03174	NO	
8	-.2671E-03	.1734E-02	-.2704E-17	-.11202	YES	-.142 E+11
9	-.5772E-03	.17-7E-.2	-.4657E-17	-.15-02	YES	-.2142E+11
10	-.9430E-03	.1604E-02	-.3666E-17	-.16505	YES	-.204 E+11
11	-.7355E-03	.1727E-02	-.6226E-17	-.26201	YES	-.328 E+11
12	-.5062E-03	.1704E-02	-.6585E-18	-.02002	NO	